Desalination and Water Treatment
www.deswater.com

doi:10.5004/dwt.2019.24516

165 (2019) 253–268
October

A green approach for iron removal and subsequent phosphate removal in Al Kharga (Egypt) using date palm biochar and its re-usability: Case study

Dalal Z. Husein

Chemistry Department, Faculty of Science, New Valley University, Al-Kharga 72511, Egypt, email: dalal_husein@scinv.au.edu.eg, dalal_husein@yahoo.com (D.Z. Husein)

Received 8 December 2018; Accepted 9 June 2019

ABSTRACT

Al Kharga Oasis is a rural area and depends on agricultural activities and date palm cultivation in particular. In Al Kharga, the only source for all water activities is the groundwater that shows an abnormal concentration of iron ions. In this study, four parts of palm wastes: palm coir, palm leaflets, date empty bunches, and date stone were used to prepare biochars in a green approach. Palm biochars were used to remove elevated iron content from groundwater in column modes to explore the most effective part. The prepared palm coir biochar exhibited excellent affinity towards iron ions due to its high surface area, 702 m^2/g, and loading capacity, 7.71 mg/g. The spent iron-loaded palm coir biochar was used then to remove phosphate ions from water. The loading capacity of for phosphate uptake was found to be 6.4 mg/g. Iron adsorption could be controlled by many processes because the correlation coefficient values of Langmuir, Freundlich and Temkin isotherms were close to one another. The Freundlich model was observed to be the best fit among other models for phosphate removal. The pseudo-second-order model has been observed to simulate iron and phosphate adsorption processes. The reusability and adsorption mechanisms of iron and phosphate adsorption by palm biochar have been discussed. The study revealed that palm waste biochar could be used as a practical and low-cost adsorbent for the removal of iron and phosphate ions because of their easy regeneration and high adsorption capacity.

Keywords: Iron removal; Phosphate; Successive adsorption; Biochar

1. Introduction

Iron and phosphate are commonly found in surface water. According to Egyptian standards for drinking water, iron content should not exceed the maximum level of 0.3 mg/L while phosphate ions should not exist in drinking water. The presence of iron in drinking water at elevated concentrations can cause health problems [1]. The occurrence of phosphate in drinking water considered as an indication for water pollution. Therefore, excess iron and phosphate need to be removed from drinking water. Iron removal from water is most commonly carried out by ion exchange and water softening [2], supercritical fluid extraction [3], limestone treatment [4], oxidation by aeration, ozonation, chlorination, followed by filtration [5] by aerated granular filter [6] and by adsorption [7]. Aeration is the most common method for iron removal from groundwater, which is however not so popular at domestic level [8]. Regarding phosphate removal, various techniques have been employed, including constructed wetlands [9] and biological nutrient removal methods [10].

Safe drinking water must be available to all communities, rural and urban areas, worldwide. Unfortunately, water infrastructure is poorly developed in many rural areas located in Egypt, or non-existent. Al Kharga Oasis has one of the oldest and longest continuous records of groundwater using by a human being in the world [11]. Al Kharga Oasis; one of the largest oases in Africa; is the capital of the New Valley Governorate and includes the western desert of Egypt. The only source for all water activities is the groundwater that extracted from the Nubian sandstone aquifer. The non-renewable Nubian Sandstone Aquifer System extends

*Corresponding author.

under the New Valley area and is shared among Egypt, Sudan, Libya, and Chad. The aquifer covers a total area of about 630,000 km^2 and reaches to a depth of 3.5 km below the surface in some areas [12]. The recharge of the Nubian sandstone aquifer is thought to be negligible [13]. Although the aquifer is a huge water resource, the groundwater level in Al Kharga has been severely decreased and the aquifer is deeply vulnerable to deterioration due to recent agricultural and industrial activities development [14]. The over-exploitation of aquifer groundwater recorded a large drop in groundwater heads reached from 70 to 80 m as the rate of groundwater extraction exceeds the average rate of aquifer recharge. The water quality of the aquifer shows abnormal concentration for iron ions. Iron content reaches to 10 mg/L in some wells [15]. As a result of such very high iron content, rust-colored deposits and a brown slime produced and build upon good screens, pipes, and plumbing fixtures. Although iron is an important element for a various biological process in human and all living organisms, elevated concentration of iron cause severe health issues. Because of its limited capacity to excrete, it accumulates in organs like the liver, heart, and pancreas causing damage to such tissues. Due to the vigorous oxidizing nature of iron, serious health issues such as liver cancer, diabetes, cirrhosis, cardiac arrhythmias, Alzheimer's disease, bacterial and viral infections, is occurring when the iron content is higher than 0.3 mg/L (as set by international and Egyptian standards for drinking water).

Another issue on the top of environmental problems in Al Kharga oasis is the solid waste accumulation due to palm trimming. In Al Kharga, there are about 62459 palm trees that generate total solid wastes of about 36147 tons annually [16]. Trimming of palm trees is an important process to increase fruit production. Accumulation of wastes generated from the trimming of palm trees causes a serious environmental issue with this waste material acting as potential fuel for any fires that might occur and as bait for disease-causing insects [17]. Attempts of people to dispose of the palm trimming wastes by burning at their locations, without following the safe methods and precautions required in these cases lead to many severe environmental issues. Thus, there is an urgent need to find a suitable solution to avoid environmental issues and utilize these solid wastes as value-added materials.

Date palm (Phoenix dactylifera L.) is one of the most important non-wood renewable resources that are lignocellulosic material. An adult date palm tree (Fig. 1) has a stem or a trunk of 15–25 m high and leaves or frond. Each frond has about 150 leaflets which can be up to 30 cm in length and 2 cm in breadth. Leaves look like feathers with 3–5 m long. Each palm tree bears 6–10 fruit bunches and 12–15 new leaves are formed and trimmed, under normal conditions, annually. Using renewable, low-cost and locally abundant lignocellulosic materials in the removal of pollutants get great attention [18]. Palm wastes can be considered as one of the best candidates for the removal of pollutants due to its high carbon content and availability [19].

One of the challenges in the production of low-cost biochar is prepared with a large surface area. The main objective of this study is: (a) transforming the palm trimming wastes to value-added product; biochar; that is prepared in a green approach, (b) characterization of the produced biochars, (c) application of the prepared material to remove elevated iron concentration from drinking water samples in Al Kharga, (d) explore the most effective part of the palm tree to remove iron in fixed bed technique, (e) using of spent iron-loaded biochar in the removal of phosphate from natural water and (f) regeneration of the exhausted biochar beds to evaluate iron and phosphate recycling efficiency.

Fig. 1. Parts of date palm tree.

2. Methods and materials

2.1. Location map, sampling, and preservations

Al Kharga is situated in the tropical, arid climate zone and is considered as one of the driest areas on Earth [20]. Economically, Al Kharga depends mainly on agricultural activities and date palm cultivation in particular. Seven drinking water samples were collected from tap water in houses and named as A, B, C, D, E, F, and G. Fig. 2a shows a location map of the study area and sites of drinking water samples which cover a distance of about 8.94 Km^2. The sampling and preservations performed as recognized for drinking water sampling and preservations standards in the Standard Methods for the Examination of Water and Wastewater [21]. The physicochemical characteristics of collected drinking water samples, such as pH, dissolved oxygen (DO), electrical conductivity (EC), total dissolved solids (TDS), total alkalinity and total hardness, were determined. For dissolved iron determination, the samples were filtered through a 0.45 µm membrane filter at the time of sampling. Then, the samples were stored in polyethylene bottles at 4°C to avoid iron biodegradation until the time of adsorption studies.

2.2. Biochars preparation and characterization

Samples from different parts of a date palm namely palm coir (PC), palm leaflets (PL), date empty bunches (DB) and date stone (DS) were collected from the Faculty of Education garden site (Lat. 25.442804, Long.

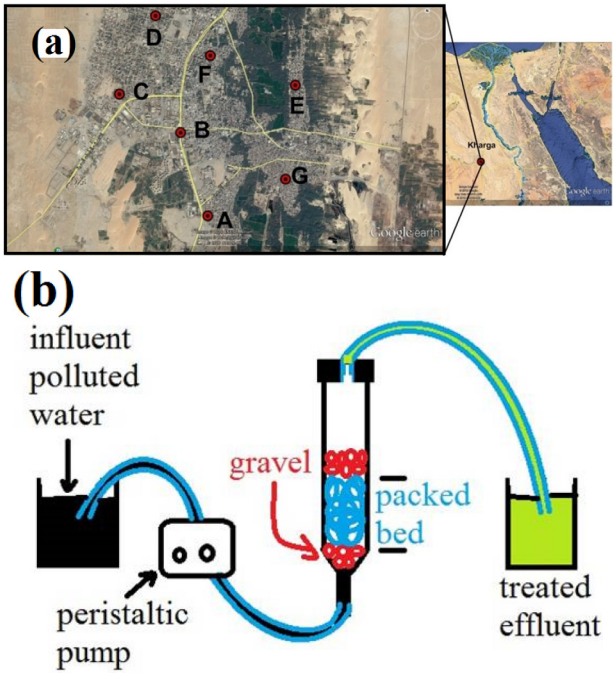

Fig. 2. Location map of study area (a) and scheme of the fixed bed column adsorption system (b).

30.542808), Al Kharga. Collected raw materials were cut into small pieces, oven dried and ground using a home mixer. The powder is screened to have a particle size less than 125 µm. Five grams of raw date palm powder was covered with deionized water and subjected to microwave (domestic microwave oven, Samsung, 2450 MHz, 800 W) radiation for 2 min. This step is important to remove soluble hemicelluloses and lignin via thermal pretreatment [22]. After cooling, the residue is filtered, dried at 65°C then subjected again to microwave radiation under minimal oxygen to carbonize to biochar. The required time for carbonization depends on the part of the palm tree. PC, PL, DB, and DS take about 2, 3, 4.5 and 8 min, respectively, to be in carbonized form, PCC, PLC, DBC, and DSC.

The prepared palm biochars were characterized using different techniques. Carbon, hydrogen, and nitrogen contents were performed in obtaining powder using a CHN Elemental Analyzer (2400 Series II, Perkin Elmer, USA) while the oxygen content of the samples was calculated by difference. FTIR analysis was performed using (Jasco FTIR 310, Japan) to analyze the functional groups of palm residues with the KBr disk technique. The surface area and pore volume of biochars were measured by nitrogen adsorption/desorption at 77 K using the BET method (ASAP 2000, Micromeriticsue, USA). For drinking water samples, pH, conductivity, TDS and DO were measured using a multi-parameter device (Inolab multilevel WTW, Germany). Total hardness and alkalinity were measured using the burette titration method. Iron concentration was measured using flame atomic absorption spectrometer (Perkin Elmer-100). The phosphate concentrations in the output solution were measured by IC- Dionex 2500.

The exhausted bed, PCC, used in iron-synthetic solution experiment was collected and washed with deionized water to remove excess iron ions. Then the iron-loaded biochar, Fe-PCC, was dried at 85°C for 6 h prior to using in the phosphate removal process. The morphology of the PCC and Fe-PCC were taken using a JEOL JSM 6360 LV electron Microscope while the X-ray diffraction (XRD) pattern of Fe-PCC was performed using a Phillips; PW 1710 Diffractometer with CuKα radiation of wavelength 1.5418 A^0.

2.3. Adsorption studies

2.3.1. Iron removal from drinking water and regeneration

Continuous adsorption studies were carried out in a glass column provided with a porous glass plate with an inner diameter of 1.2 cm and a height of 10 cm, Fig. 2b. The column was filled carefully with date palm biochar between two supporting layers of gravel (about 3 cm).The bed depth of palm biochar was 4 cm (1.8 g). The drinking water of the highest iron content, sample A, was pumped using a peristaltic pump (Watson Marlow make) upward. The effluent was collected at regular intervals for analysis from the top of the column. The synthetic solution was prepared by loading the deionized water with iron ($FeCl_3$) content as detected in the drinking water sample. The feed influent flow rate was maintained at a constant value through the column (Q = 3 mL/min). The iron content of the output solution was measured at selected time intervals. The pumping was continued till there was no further adsorption, i.e., the iron concentration at the influent and effluent remained unchanged. A regeneration cycle was performed with a 4% HCl solution after each adsorption cycle service (3 cycles in total). The exhausted bed was charged using 4% HCl solution with the same upstream flow rate until the iron concentration in the effluent reached 0.1%.

The adsorption kinetics and isotherms experiments were performed in batch mode and were performed by mixing 0.1 g of PCC biochar with 20 mL of iron solution (10–75 mg/L). The sorption mixture was agitated (150 rpm) till equilibrium at room temperature.

2.4.2. Phosphate removal and regeneration

The removal of phosphate in fixed bed mode was performed under the same operational conditions as carried out in iron removal experiments. The phosphate content in drinking water was detected only in sample G with phosphate concentration of 0.42 mg/L. Thus water sample in site G was chosen to explore the applicability of iron-loaded biochar to treat real water. The phosphate-containing model solution was prepared by loading the deionized water with the same phosphate (KH_2PO_4) concentration of the surface water sample. The bed depth and flow rate for phosphate removal experiments kept fixed as performed in the case of iron removal. Regeneration of biochar was performed by using a 4% NaOH solution with the same upstream flow rate until the phosphate concentration in the effluent reached 0.1%.

In batch mode, the kinetics and isotherms experiments were performed by mixing 0.1 g of iron-loaded PCC biochar with 20 mL of phosphate solution (10–40 mg/L) at different

time intervals. The sorption mixture was shaken at a speed of 150 rpm and the equilibrium time was 6 h.

3. Results and discussion

3.1. Characterization of biochars (Elemental, FTIR and BET analyses)

The determined C, H, N, and O (by difference) are recorded in Table 1. For raw palm residues, the carbon content is ranged from 47.33% to 45.99%, while the carbon content increase to a range of 67.46–65.04 % after carbonization. This phenomenon is attributed to the volatilization of both H and O atoms from the raw carbon matrix during the carbonization process which results in presence of new pores and increases surface area and pore volume. Date palm wastes were characterized by higher ash percentage [23]. Palm leaflets recorded the highest ash content of 8.01% and the lowest carbon content of 45.99%. Palm coir, have the highest carbon percentage of 47.33%, Tables 1 and 2. The results showed that the highest yield was recorded for PCC, while the lowest value was recorded for PLC. Surface area, total pore volume, micro pore volume and average pore diameter of biochars are presented in Table 2. The four carbonized samples show high proportion of micro pore volume (about 90% of total pore volume) which means that carbonized palm residues, PCC, PLC, DBC, and DSC have wide micro pores and small mesopores.

Table 1
Elemental analysis of raw waste and biochars of palm residues (Oxygen was estimated by difference)

Sample	C%	H%	N%	O%
PC	47.33	6.06	0.3	46.31
PCC	67.46	2.94	1.42	28.18
PL	45.99	6.04	0.72	47.25
PLC	65.63	3.14	1.85	29.38
DB	46.03	6.85	0.26	46.86
DBC	65.04	3.97	0.61	30.38
DS	47.12	6.49	1.18	45.21
DSC	67.38	3.15	2.38	27.09

Table 2
BET surface area, total pore and micro pore volume, ash and yield of prepared biochars

Biochar	BET surface area (m^2/g)	Total pore volume (cm^3/g)	Micro pore volume (cm^3/g)	Average pore size (A°)	Ash	Yield %
PCC	702	0.34	0.31	19.37	2.63	39.31
PLC	612	0.29	0.26	18.95	8.51	36.84
DBC	644	0.32	0.29	19.88	2.06	37.73
DSC	679	0.33	0.3	19.44	2.24	38.84

FTIR spectra, Fig. 3, of the raw palm wastes showed three main absorption bands at 1700, 1600 and 1425 cm^{-1} which attributed to the stretching modes of C=O, conjugated C=C and the stretching vibrations of C-C bonds, respectively. Reduction or disappearance of such bands in PCC, PLC, DBC and BSC spectra is evident for carbonization. For raw palm materials, the stretching modes of C=O bonds can be seen around 1090 cm^{-1}. The appeared aliphatic C-H bond at 2900 cm^{-1} suggests the presence of hemicellulose and cellulose, which are reduced in biochars, PCC, PLC, DBC, and DSC. Such a decrease in the aliphatic C-H band suggests an increasing of aromatization and decreasing of nonpolar aliphatic fractions. The absorption band at 1600 cm^{-1} in raw materials attributed to C=O of ketons and carboxyl or C=C aromatic components weakened in biochars because C=O was easy to rupture to form gas products. The peak appeared at 3400 cm^{-1}, may correspond to the stretching of the O-H functional group and this indicates the presence of bonded hydroxide in the raw samples. The reduction of such beak upon carbonization suggests a loss of OH-containing aliphatic compounds. As shown by the FTIR spectra, the carbonization process modifies the oxygenated functional groups of palm wastes due to the loss of carboxyl, ether and phenolic groups, whereas more ϖ-conjugated aromatic structures were formed.

3.2. Physicochemical characterization of drinking water in the study area

It is essential to measure physio-chemical parameters such as pH, conductivity, TDS, total alkalinity, total hardness and dissolved oxygen to give an idea about the water quality. All results were presented by Surfer 8 program.

3.2.1. pH and dissolved oxygen (DO)

Generally, low pH values raise the corrosive nature of water and there is a positive correlation with conductivity and total alkalinity. Most of the biological and chemical reactions in the human body are influenced by the pH of water system. For investigated samples, the pH values varied from 7.15 to 7.37, Fig. 4a, and found within the lim-

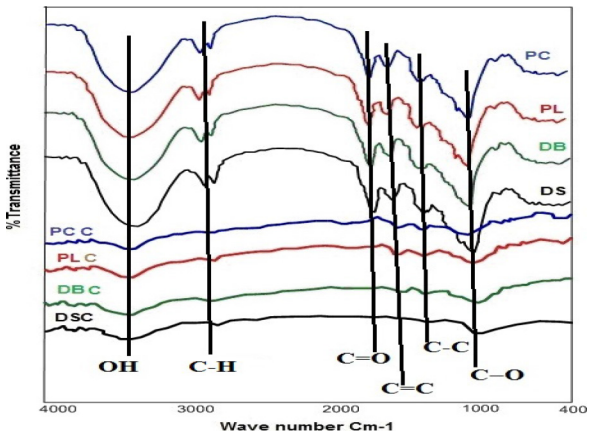

Fig. 3. FT-IR analysis of palm tree residues, before and after carbonization.

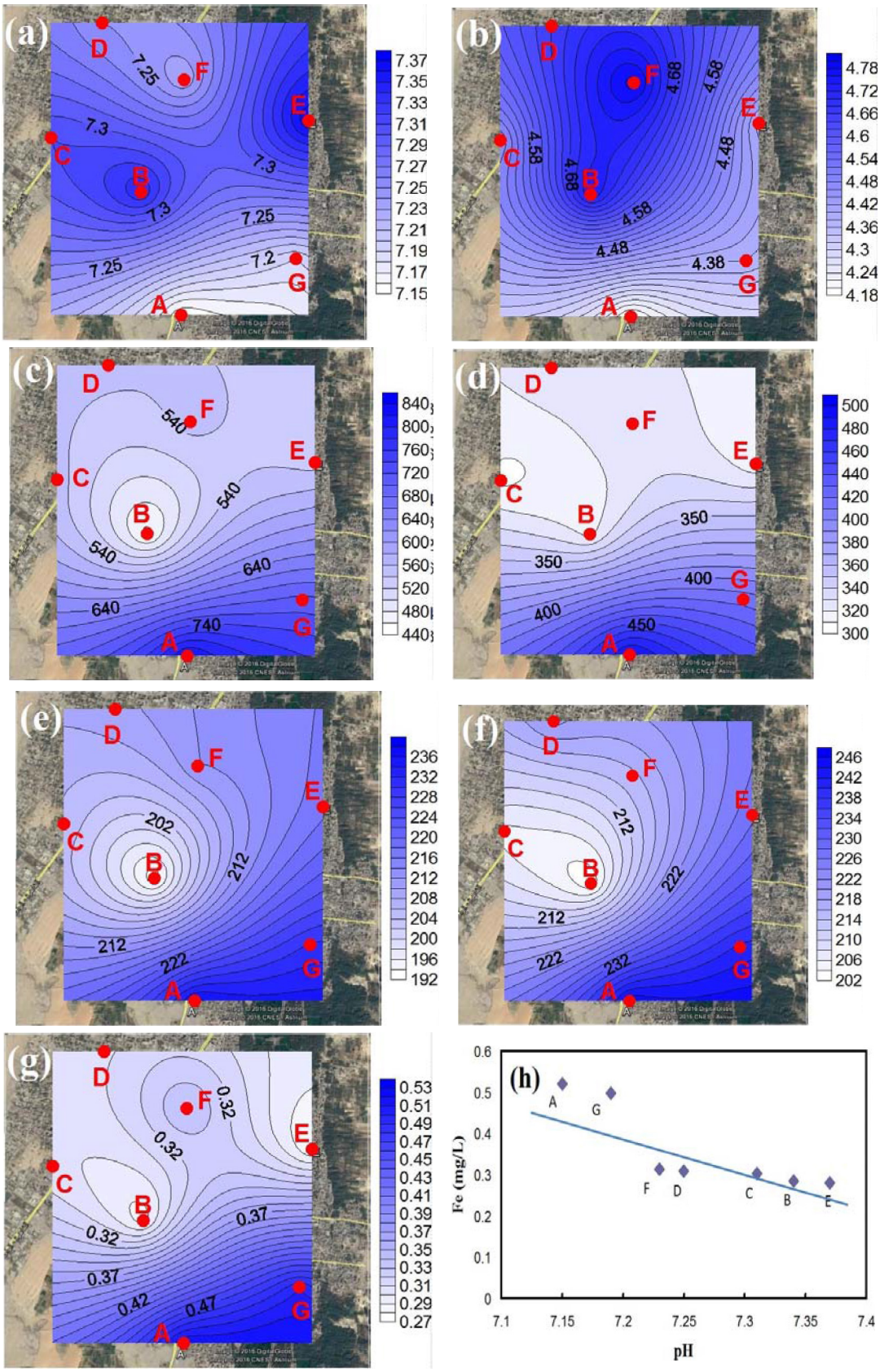

Fig. 4. Distributions of pH (a), DO (b), conductivity (c), TDS (d), total alkalinity (e), total hardness (f) and iron (g) in study area and pH-iron content relation (h).

its prescribed by WHO and Egyptian standards [24] as pH from 6.5 to 8.5 is considered satisfactory for drinking water. Dissolved oxygen (DO) is one of the most important parameters as its value gives direct and indirect information about water quality e.g. bacterial activity, photosynthesis and availability of nutrients [25]. DO value of 5 mg/L is set by WHO as the ideal standard. Sampling sites show DO values between 4.19 and 4.79 mg/L. The north area has high DO values, i.e., less polluted area (Fig. 4b). The higher value of DO can improve the taste of drinking water to be good [26].

3.2.2. Electrical conductivity (EC) and total dissolved solids (TDS)

Electrical conductivity (EC) is the measure of water capacity to conduct electric current and this capacity depends on the ionic mobility, temperature, and concentration of ions. Thus it signifies the amount of total dissolved salts or solids of water. The electrical conductivity of all the seven places is not in the allowable limits prescribed by WHO (300 µs/cm), Fig. 4c. TDS indicates the salinity behavior of groundwater and it is related to inorganic and organic substances in water. Drinking water containing more than 500 mg/L of TDS is not considered desirable as set by WHO. The most desirable limit of TDS is 500 mg/L and the maximum permissible limit is 1200 mg/L as prescribed by Egyptian standards. Higher concentration of TDS may cause gastrointestinal irritation to human and animals. The prolonged use of such drinking water may result in heart attack and formation of kidney stones. The TDS values ranged from 308 to 494 mg/L, i.e., all samples recorded acceptable TDS values, Fig. 4d. For both EC and TDS, southern part of studied area showed the highest values. As recorded in literature [27], the water quality of studied area belongs to fresh water with good water quality (as TDS < 1000 mg/L and 250 < EC < 750 mg/L).

3.2.3. Total alkalinity (TA) and total hardness (TH)

Alkalinity, hardness, and pH affect the toxicity of many water contents. Alkalinity primarily composed of carbonate and bicarbonate and has an important role in stabilizing the pH value of water. The desirable alkalinity value is prescribed as 200 mg/L by WHO for drinking water while the maximum permissible limit is 600 mg/L. For groundwater samples collected from the study area, water alkalinity was within the accepted level of WHO samples. Highest alkalinity value was recorded for the east-southern part of the studied area as indicated in Fig. 4e. The total hardness is an important parameter for evaluation of water quality. TH increases the boiling point of water and conveys if the water can be used for domestic, industrial or agricultural purposes as it prevents the lather formation with soap. The maximum permissible limit of total hardness set by WHO for drinking purposes is 600 mg/L. However, total hardness more than 300 mg/L may cause heart and kidney problems. As shown in Fig. 4f, the total hardness in samples under investigation ranged from 206 to 246 mg/L. The total hardness values of all seven water samples are within the permissible limit. It is clear that the distribution of TH and TA has the same trend as the eastern southern part showed the highest values. Depend on the total hardness value, the water quality of the study area can be classified as hard water (200 < TH < 300).

3.2.4. Iron content

As illustrated in Fig. 4g, the distribution of iron concentration shows a gradual increase toward the southeastern part of the area under investigation. All samples, except sample B, exceed the permissible limit. Such high iron concentration reflects dissolution and active leaching of iron-bearing deposits rich in aquifer materials.

There is a relation between pH value and iron concentration as solubility and availability of iron in water increases as pH value decreases. Fig. 4h shows the relation between the pH value and iron content. It is obvious that the iron content in groundwater samples increases with decreasing its pH values. For groundwater samples, the pH values range from 7.15 to 7.37 which are suitable for the growing of iron bacteria. Such bacteria oxidize soluble ferrous iron to insoluble ferric iron which considered the main source for well screens and filters clogging. Iron bacteria combine dissolved iron with oxygen to form rust-colored deposits and produce a brown slime. Iron bacteria in groundwater wells do not cause health problems, but they can reduce the yields of wells by clogging screens, filters, and pipes.

As seen in Fig.4, the southern part of the location area showed high contents of TDS, total alkalinity, total hardness and iron in drinking groundwater samples. Accordingly, the water quality of A and G samples are low compared to other samples. Such significant variability in the physicochemical composition of drinking water samples can be attributed to many factors such as water hydraulic conditions in the network, pipes material, scales in pipes, pipes age and network structure. The increase in iron concentration at the study area may indicate corrosion of pipelines.

3.3. Iron removal using different date palm biochars in fixed bed mode

The loading behavior of iron onto date palm biochars was shown by analyzing the effluent concentration vs. time or volume curves, i.e., breakthrough curves. The breakthrough curve is usually expressed as the measured concentration divided by the inlet concentration (C_t/C_0) as a function of time (t) or volume of effluent (V_{eff}) for a given bed depth (Z). The breakthrough time (t_b) whereas the iron concentration in the influent reached 10%. The bed exhaustion time (t_e) whereas the iron concentration in the effluent reached 98 % of the initial iron concentration, was used to express the parameters. The effluent volume, V_{eff} (mL), can be calculated as given below [28]:

$$V_{eff} = Q \cdot t_{total} \quad (1)$$

where Q is the influent flow rate (mL/min) and t_{total} is the total flow time (min). The value of the total iron mass that adsorbed by palm biochar, q_{total} (mg), in the column can be calculated from the area under the breakthrough curve as follow:

$$q_{total} = \frac{q}{1000}\int_{t=0}^{t=total} C_{2d}\,dt \quad (2)$$

where C_{ad}, mg/L, is the concentration of adsorbed iron (mg/L) by palm biochar.

The maximum capacity of the palm biochar column, q_e (mg/g), is calculated as shown below:

$$q_e = \frac{q_{total}}{m} \quad (3)$$

where m (g) is the dry weight of palm biochar adsorbent in the fixed bed column. The total amount of iron sent to the column (m_{total}) is calculated from the mathematical expression [29]:

$$m_{total} = \frac{C_0 Q t_{total}}{1000} \quad (4)$$

The column performance, Y%, can be evaluated by the total iron removal percentage from the ratio Y% as:

$$Y\% = \left(\frac{q_{total}}{m_{total}}\right)\times 100 \quad (5)$$

The adsorption of iron by palm biochar was carried out for drinking water sample of highest iron content, site A. Under the same conditions of 3 mL/min flow rate and the same natural drinking water, the breakthrough curves of the different parts of palm tree biochars show different behaviors. As shown in Fig. 5a, the sharper breakthrough curves, the low iron uptakes, and removal yields were obtained. The breakpoint time and total adsorbed iron quantity decreased with the following sequence: PCC > DSC > DBC > PLC, Table 3. The total absorbed iron mass and the maximum iron uptakes followed the same order. Such order is consistent with the carbon content order, as PCC contains the highest amount of carbon among all palm tree parts. The column performance, Y%, was 86.64%, 84.06%, 82.85% and 80.15% for PCC, DSC, DBC, and PLC, respectively. Column performance was the best in the case of using PCC as a fixed bed. According to EBT analysis, PCC showed the largest surface area among the different parts of the palm tree. The fixed bed column test results in Fig. 5a demonstrated that high breakthrough volumes were observed for iron uptake by palm biochars, which assigned the strong attraction of palm biochar towards iron ions under dynamic conditions.

A synthetic solution contains the same iron content of natural drinking water under the same flow rate, of 3 mL/ min was used as influent. The column performance was explored using a PCC bed. The breakthrough time of the column for iron adsorption in the model water was greater than in the natural sample (Fig. 5b). The adsorption capacity of iron increased from 7.71 mg/g in the natural drinking water to 9.49 mg/g in the model water, representing a 23% improvement, Table 4. The iron removal increased from 86.64% in natural drinking water to 94.1% in synthetic water, while the treated effluent volume of the column (V_{eff}) increased from 24.1 L to 27.3 L, which was a 13% increase. Such results demonstrated that ionic species contained in the natural drinking water considerably decrease and compete with the sorption of iron onto the PCC bed column.

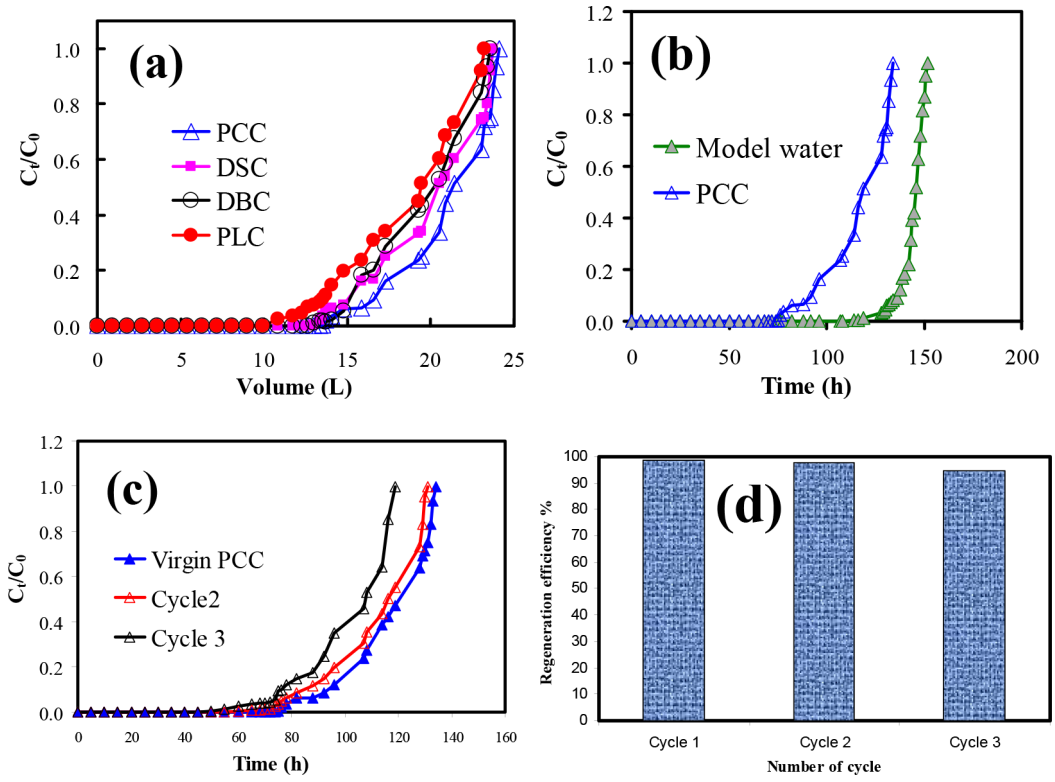

Fig. 5. The breakthrough curves of iron removal by different parts of palm tree biochars (a), removal in synthetic and natural water, effect of regeneration on PCC bed (b) and influence of regeneration efficiency (%) by cycle number (d).

Table 3
Column parameters and breakthrough time points for iron adsorption by different parts of palm tree in natural drinking water sample

Adsorbent	t_b (h)	t_e (h)	V_{eff} (L)	q_{total} (mg)	m_{total} (mg)	q_e (mg/g)	Y%
PCC	75.50	133.90	24.12	12.33	14.23	7.71	86.64
DSC	72.53	131.64	23.94	11.78	14.02	7.36	84.06
DBC	71.66	130.84	23.67	11.53	13.91	7.20	82.85
PLC	58.05	128.92	23.40	10.98	13.70	6.86	80.15

Table 4
Column parameters of iron removal by PCC fixed bed from natural drinking water and model water

Exp. parameter	t_b (h)	t_e (h)	V_{eff} (L)	q_{total} (mg)	m_{total} (mg)	q_e (mg/g)	Y%
Natural drinking water	75.5	133.9	24.12	12.33	14.23	7.71	86.64
Model water	117.2	152.1	27.36	15.19	16.14	9.49	94.10

3.4. Effect of regeneration on the iron adsorption capacity in fixed bed technique

The regeneration performance of palm biochar (PCC) was evaluated in terms of breakthrough time (t_b) and regeneration efficiency described as follows:

$$\text{Regenerated efficiency } (RE)\% = t_b(\textit{regenerated bed}) \times 100 / t_b(\textit{virgin bed}) \quad (6)$$

Regeneration attains elution of bound iron cations and restoration the surface of palm biochar for the next service step. Three cycles were carried out after regeneration the exhausted PCC with 4% HCl. After the first cycle, iron adsorption capacity of regenerated PCC is lower than that of virgin PCC. This causes the early breakthrough for regenerated PCC fixed bed column, Fig. 5c. As illustrated in Fig. 5c and d, although the sorption capacity of the PCC bed diminished after each adsorption/regeneration cycle, the PCC bed continued to have an acceptable adsorption performance for iron.

It is worth notable that no major decrease in regeneration efficiency, Fig. 5d, was observed. After one cycle, the overall adsorption capacity for PCC was well restored, as it slightly decreased by only 1.9% and during the subsequent cycle, the iron adsorption capacity difference was significantly observed (5.2%). However, the efficiency of regeneration for the second and third cycle was 97.9% and 94.7%, respectively, suggesting that palm coir carbon (PCC) can be reused many times and can treat large volumes of drinking water. This is because column performance provides multiple repetitions of service and regeneration cycles. Such finding has been also confirmed by a slightly decrease in V_{eff}, m_{total} , q_{total} and other parameters listed in Table 5.

3.5. Iron removal using PCC biochar in batch mode: kinetics, effect of time, initial concentration and isotherms

To describe the adsorption process, kinetics and isotherm studies were performed in batch mode. The adsorption capacity, q_e (mg/ g) of PCC biochar towards iron was calculated as:

$$q_e = \frac{(C_o - C_e)V}{m} \quad (7)$$

where C_0 and C_e are the initial and equilibrium iron concentration, m is the PCC mass (g) and V is the volume of iron solution (mL).

The kinetic study was performed to justify the rate at which the PCC biochar adsorbed iron cations. The iron-adsorption kinetics is illustrated in Fig. 6. The mononuclear and binuclear adsorption processes were explained by the pseudo-first-order [30] and pseudo-second-order [31] kinetic models. The contribution of desorption process was described by the Elovich [32] model. In addition, the intraparticle diffusion [33] kinetic model was investigated:

$$Log(q_e - q_t) = \log\ q_e - \left(\frac{K_1}{2.303}\right)t \text{ Pseudo-first-order model} \quad (8)$$

$$\frac{t}{q_t} = \frac{1}{(K_2 q_e^{\,2})} + \left(\frac{1}{q_e}\right)t \text{ Pseudo-second-order model} \quad (9)$$

Table 5
Column parameters for palm biochar PCC backed column, effect of regeneration

Exp. Parameter	t_b (h)	t_e (h)	V_{eff} (L)	q_{total} (mg)	m_{total} (mg)	q_e (mg/g)	RE%
Cycle 1	74.35	132.93	23.98	12.92	14.03	7.56	98.48
Cycle 2	73.94	130.2	23.58	11.9	13.91	7.44	97.93
Cycle 3	71.56	127.8	23.04	10.91	13.59	6.82	94.78

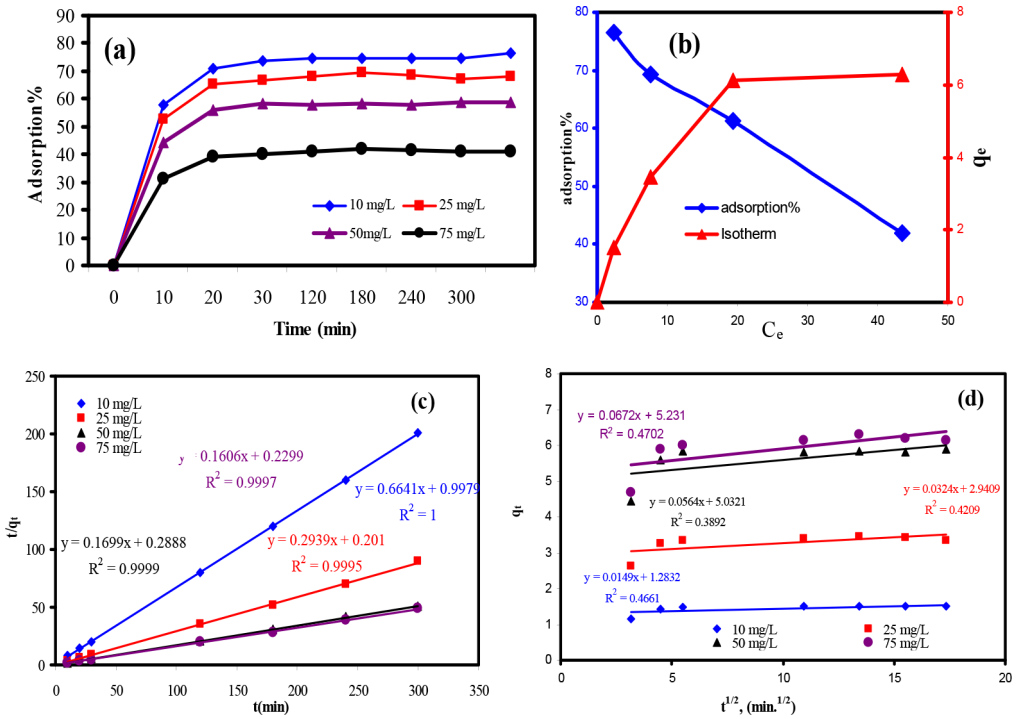

Fig. 6. The adsorption of iron by PCC biochar in batch mode, effect of time (a), effect of initial iron concentration and isotherm (b), psuedo second order kinetic model (c) and intra particle model (d).

$$q_e = C + K_{\text{int}} t^{1/2} \text{ The intraparticle diffusion model} \quad (10)$$

$$q_t = \frac{1}{\beta}\ln(\alpha\beta) + \left(\frac{1}{\beta}\right)\ln t \text{ Elovich model} \quad (11)$$

where q_e and q_t represent iron adsorption capacity (mg/g) of PCC at equilibrium and at time t (min), respectively. K_1 (min^{-1}), K_2 (g mg^{-1} min^{-1}) and K_{int} are the pseudo-first-order rate constant, the pseudo-second-order rate constant and intraparticle rate constant, respectively. C (mg g^{-1}) is related to diffusion resistance, α (mg kg^{-1}) is the initial adsorption rate, and β (kg mg^{-1}) is the desorption constant.

Adsorption of iron by PCC is dependent on contact time. As shown in Fig. 6a. A rapid increase during the beginning was observed, in which the equilibrium plateau was achieved after 30 min of contact. With increasing concentration of iron solution, q_e increased, while adsorption % decreased (Fig. 6b). At low initial iron concentration, the availability of active adsorption sites and the biochar surface area were relatively high, and the iron cations were easily removed. At higher initial iron concentration, the total available active sites are limited, therefore resulting in a decrease in adsorption% of iron. The increased adsorption capacity, q_e, at higher initial iron concentration can be assigned to the enhanced driving force.

Quantitative evaluation of the four kinetic models was done by comparing the relative correlation coefficients (R^2), Table 6. The results revealed that the sorption process that best fits the experimental data was the pseudo-second-order kinetic model ($R^2 > 0.999$). The amount of iron adsorbed at equilibrium calculated from the pseudo-second-order model and the obtained experimental values were found to be close (Table 6, Fig. 6c). Such finding confirms fitting of the pseudo-second order kinetic model to Fe/PCC adsorption experiment and, consequently, in the control of adsorption rate an activated adsorption or chemisorption mechanism must be involved. The results also show that the intra particle diffusion mechanism is not the only limiting step as the lines of the q_t against $t_{0.5}$ graph for iron removal by PCC do not pass through the origin, Fig. 6d. Thus, other external interaction mechanisms (surface adsorption and liquid film diffusion) must be acting simultaneously. The Elovich model explains the heterogeneous film diffusion process, which is controlled by the diffusion factor and reaction rate. Although the Elovich model showed a bad fit with the experimental data, it can be concluded that the adsorption process is not a simple first-order reaction. The adsorption of iron onto PCC biochar is an integrative process that is consistent with the pseudo-second order kinetics model.

The equilibrium adsorption isotherms are important to verify the adsorption mechanism and to define the relationship between iron and PCC biochar. To investigate the adsorption process, Langmuir [34], Freundlich [35] and Temkin [36] isotherms are used to analyze the experimental data:

$$\frac{C_e}{q_e} = \left(\frac{1}{q_L K_L}\right) + \left(\frac{1}{q_L}\right) C_e \text{ Langmuir isotherm} \quad (12)$$

$$Log q_e = \log K_F + \left(\frac{1}{n}\right)\log C_e \text{ Freundlich isotherm} \quad (13)$$

Table 6
The kinetic parameters for iron adsorption by PCC biochar

C_0	q_e (mg/g) (experimental)	q_e (mg/g) (calculated)	Pseudo-first-order	Pseudo-second-order	Elovich	Intra particle diffusion
10 mg/L	1.53	1.51	K_1 = 0.01	K_2 = 0.442	α = 0.985	K_{int} = 0.168
			R^2 = 0.554	R^2 = 1	β = 1.12	C = 8.49
					R^2 = 0.606	R^2 = 0.466
25 mg/L	3.46	3.40	K_1 = 0.008	K_2 = 0.430	α = 4.3×10^3	K_{int} = 0.193
			R^2 =0.136	R^2 = 1	β = 0.97	C = 11.16
					R^2 = 0.576	R^2 = 0.421
50 mg/L	6.13	5.39	K_1 = 0.008	K_2 = 0.1	α = 13.94×10^5	K_{int} = 0.152
			R^2 =0.399	R^2 = 1	β = 1.23	C = 15.5
					R^2 = 0.528	R^2 =0.389
75 mg/L	6.29	6.22	K_1 = 0.002	K_2 = 0.112	α = 25.6×10^3	K_{int} = 0.067
			R^2 = 0.332	R^2 = 0.999	β = 1.94	C = 5.23
					R^2 = 0.619	R^2 = 0.471

$$q_e = B\ln A + B\ln C_e \quad \text{Temkin isotherm} \tag{14}$$

where q_L (mg/g) is the sorption capacity of PCC, K_L (L/mg) is the Langmuir constant, K_F (L/mg) is related to PCC adsorption capacity, *1/n* is the Freundlich constant, A (L/g) is related to the equilibrium binding, and B (J/mol) is related to the adsorption heat.

Assessments of the Langmuir parameters showed very good applicability of such model for iron adsorption by PCC, Table 7. The essential feature of the Langmuir isotherm model is defined in term of equilibrium parameter, R_L:

$$R_L = \frac{1}{\left(1 + K_L C_0\right)} \tag{15}$$

where K_L is related to adsorption energy. As tabulated in Table 7, R_L was < 1 and indicated that the adsorption of iron was favorable, and the value of K_L reflects a good affinity of PCC biochar towards iron.

The adsorption of iron by PCC can also be described by the Freundlich model. The value of n is between 1 and 10, suggesting a favorable adsorption process with a higher degree of homogeneity. The Langmuir isotherm showed a slightly better fit than the Freundlich model.

The Temkin isotherm model also describes the adsorption of iron by PCC biochar (R^2 = 0.97, Table 7). Thus, electrostatic interaction between biochar and iron cations is an important mechanism.

Table 7
The adsorption isotherm parameters of iron removal by PCC biochar

Langmuir		Freundlich		Temkin	
q_L	8.53	n	1.86	A	0.92
K_L	0.10	K_F	1.06	B	1.92
R_L	0.04				
R^2	0.99	R^2	0.95	R^2	0.97

Upon the same operating conditions, the capacity of iron adsorption onto PCC in a fixed bed column (7.71 mg/g) is much higher than the capacity recorded in batch mode experiment (6.22 mg/g). This finding may be occurred due to the complete saturation of PCC active sites in the case of fixed bed mode [37]. Henriques et al. [38] and Shahbazi et al. [39] also observed this behavior.

3.6. Characterization of spent iron-loaded PCC biochar (Fe-PCC)

The exhausted Fe-PCC material was examined using XRD analysis, Fig. 7a to specify the iron phase that adsorbed into PCC biochar. The XRD pattern of iron-impregnated biochar, Fe-PCC, exhibits an amorphous halo at around 26° which is typical of amorphous nature of carbon. Also, a broad peak at 35° indicates akaganeite presence. It has been reported that two-line ferrihydrite (HFO) shows two broad diffraction peaks at 35.9°and 61.4°, corresponding to *d* spacings of 0.250 and 0.148 nm, respectively [40]. The absence of these two peaks in the XRD pattern of Fe-PCC indicates that HFO was not present. There was an inconspicuous peak at 56°, confirming the existence of akaganeit. There was no detectable peak at 2θ values of 30° to 80°, suggesting that the loaded iron on PCC biochar took the amorphous phase form, which was more valuable than crystalline iron oxides in phosphate removal. SEM images of virgin PCC before and after adsorption (Fe-PCC) of iron are shown in Fig. 7b and c. According to SEM images, the surface of PCC seems to be as a roughness structure with cavities and groves before adsorption. The surface is smoother and the roughness structure disappeared after adsorption due to the deposition of iron or a progressive change in PCC surface mineralogy.

Comparing the two FTIR spectra of virgin and iron-loaded biochars (Fig. 7d), the appearance of certain bands and disappearance of others can be observed after the conversion of biochar into Fe-loaded biochar. The main difference between FTIR spectra of virgin PCC and Fe-PCC is the emerging broad peak at 3410 cm^{-1} due to the presence

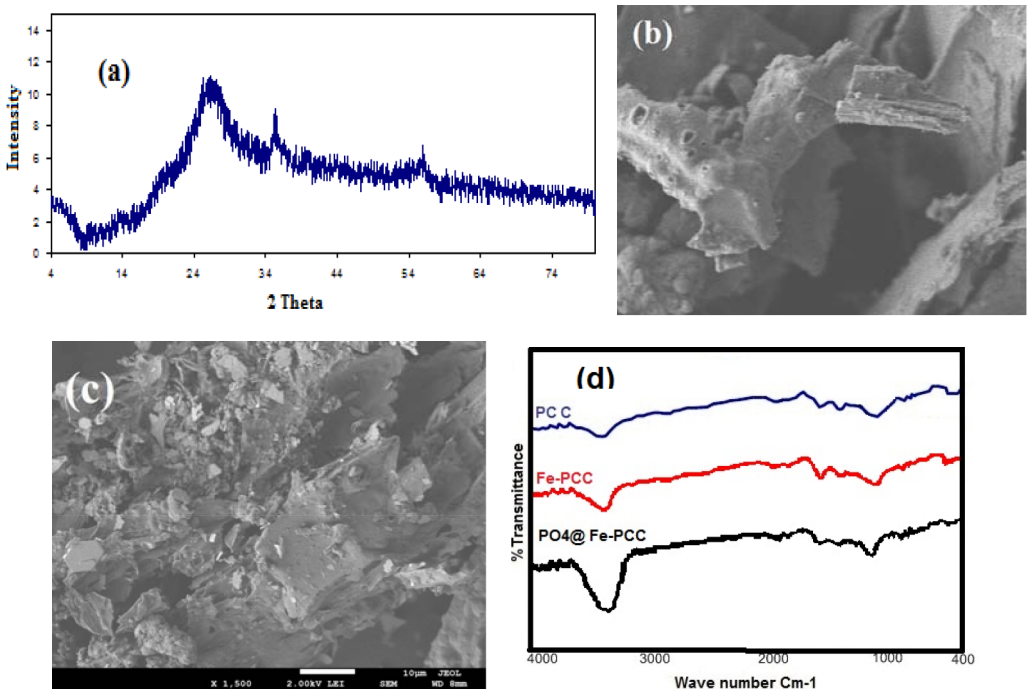

Fig. 7. XRD analysis of Fe-PCC (a), SEM images of virgin PCC (b) and Fe-PCC (c) and FTIR analysis of virgin biochar, iron-loaded, and phosphate-loaded biochars (d).

of hydroxyl groups on Fe-PCC biochar. This is probably attributed to the partial coating of the PCC biochar surface with akaganeite (FeOOH) [41]. This peak shifted from 3400 cm^{-1} in the virgin PCC to 3410 cm^{-1}, in the spectra of Fe-PCC, suggesting chemical interactions between the iron cations and the –OH groups [42]. The C=O stretching vibration at 1600 cm^{-1} is considerably enhanced and shifted to 1585 cm^{-1} after loading of biochar with iron. Compared with the raw palm waste, Fig. 3, some peaks in biochar disappeared or decreased during the carbonization, i.e., aliphatic-like, protein-like, cellulose-like substance. Therefore, the aromaticity increased in the formed biochar. Such cyclic aromatic π-systems are a weak cation- π binder and may bind with iron easily. Hence, iron-π interaction might be responsible for iron adsorption [43]. The hydroxyl and carbonyl groups on the PCC surface are responsible for the anionic and basic properties, respectively. Therefore, potentially anionic contaminants such as phosphate anions can be adsorbed onto Fe-PCC biochar's surface [44]. The carboxylic peak around 1700 cm^{-1} disappeared in the spectra of Fe-PCC indicated that –COOH functional groups have been involved in the loading of biochar with iron. The oxygen-containing functional groups play an important role in the adsorption or binding process [45]. The peak at 1090 cm^{-1} (ether linkage –C–O–C–) shifted to 1095 cm^{-1} in the spectra of Fe-PCC biochar indicated that the participation of the ether linkage in Fe adsorption. The key peak at 630 cm^{-1}, corresponds to Fe–O bond deformations; confirm the formation of akaganeite particles on the biochar surface.

3.7. Mechanism of iron adsorption onto PCC biochar

The iron adsorption onto PCC biochar was a very complicated process. Based on the results of kinetic study, the adsorption process involved chemical bonding and physical function behavior. This means the sorption process includes the intra-particle diffusion processes, surface adsorption, and external liquid film diffusion. According to the isotherm study, the adsorption mechanism of iron onto PCC refers to electrostatic interaction, also physical acting.

The FTIR analysis proved that the surface complexation (coordination) plays an important role during the adsorption or loading of iron onto biochar. The oxygen-containing functional groups (such as -OH, -CO and -COOH) participates in iron binding. The functional groups' complexation between the biochar and cationic contaminants is usually associated with the release of hydrogen ions into solution and this leads to reduction of solution pH [46]. This, in turn, results in demineralization of naturally occurring alkaline ash that was formed during biochar formation (pyrolysis). Fan et al. studied the released cations during the adsorption process and reported that more cations were released to the supernatant, especially the K^+ and Ca^{2+} ions which get involved in the ion exchange process [47]. Furthermore, the aromatic band changes in FTIR spectra revealed that iron-π interaction might be responsible for iron sorption. The aromatic π-system can act as the π-donor and such ability (electron donating) became stronger as the aromaticity increased [48]. Therefore, the mechanism between iron and PCC biochar was schematically presented in Fig. 8, involving surface functional groups complexation, electrostatic interaction, iron-π interaction, ion exchange, and others.

3.8. Removal of phosphate ions using Fe-PCC and its re-usability in fixed bed column mode

To evaluate the practical applicability of Fe-PCC biochar in the removal of phosphate from natural drinking water,

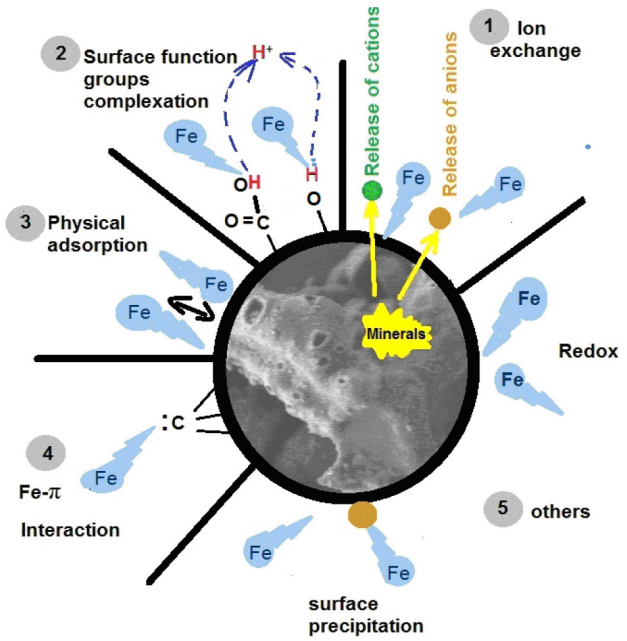

Fig. 8. Schematic illustration of iron removal by PCC biochar.

the fixed-bed column experiments were carried out at a natural occurring concentration of 0.42 mg/L phosphate, site G. Phosphate concentration in synthetic model water was like the concentration of phosphate in the natural drinking water. The pH of influent solutions was maintained at natural pH. The breakthrough curves for phosphate were obtained with flow rates of 3 m/min. As shown in Fig. 9a, very high breakthrough volumes were obtained for phosphate in both synthetic and real drinking water, Table 8. The breakthrough volume obtained for phosphate in real water was significantly higher than that of the model solution under these experimental conditions. Such an outcome may be attributed to the presence of naturally occurring cations in water such as calcium and magnesium. The regeneration efficiency (%) for the first, second and third cycles were 87.6%, 81.5%, and 73.8%, respectively, suggesting that iron-loaded palm coir carbon (Fe-PCC) can be reused many times and can treat large volumes of natural water, Table 9 and Figs. 9b and c. This study again illustrates the affinity of the palm waste biochar for phosphate and demonstrates that the synthesized biochar is suitable for purifying natural drinking groundwater in a fixed-bed system.

3.9. Adsorption of phosphate by iron-loaded palm biochar in batch mode: effect of time, initial concentration, kinetics and isotherms

As shown in Fig. 9d, the iron-loaded palm biochar displayed rapid adsorption kinetics towards phosphate ions. The time needed to reach adsorption-desorption equilibrium was 2 h. Accordingly, phosphate adsorption could be promoted by the functional interaction between Fe-PCC biochar and phosphate. Obviously, the initial high uptake is due to the abundance of free active binding sites. The mesopores on the biochar surface become almost saturated with phosphate anions during the initial stage of sorption process. Hence, the phosphate anions have to traverse deeper into the micro pores, thus leading to decrease adsorption rate and driving force.

Fig. 9e shows plots of the adsorption capacity of Fe-PCC and the percentage removal of phosphate versus the initial concentration of phosphate. It is evident that the adsorption capacity of iron-loaded biochar increases with increasing initial phosphate concentration, suggesting that a higher initial phosphate concentration can enhance the sorption process, although the adsorption % of phosphate decreases with an increase in the initial concentration. The increasing uptake capacity of Fe-PCC with increasing phosphate concentration may be attributed to higher collision probability between phosphate anions and Fe-PCC particles.

The obtained adsorption data are simulated in accordance with the pseudo-first-order, pseudo-second-order, Elovich and intra particle diffusion kinetic models to explore the adsorption mechanism of phosphate and evaluate the efficiency of the process. It was found that the pseudo-second order kinetic model better simulated the uptake behavior of phosphate ($R^2 > 0.98$), Fig. 9f and Table 10. This outcome suggested that chemisorption could be the controlling factor for the adsorption process.

As listed in Table 11, Freundlich isotherm had a higher correlation coefficient ($R^2 = 0.999$) for Fe-PCC than the Temkin and Langmuir models. This outcome suggests that heterogeneous processes control phosphate removal by Fe-PCC. However, the measured R_L value (0.11) indicated that the adsorption process is favorable. The outcomes acquired from isotherm study suggested that the predominant mechanism for phosphate adsorption by Fe-PCC is polynuclear and mononuclear adsorption onto iron-loaded palm biochar.

3.10. Mechanism of phosphate adsorption by iron-loaded palm biochar

The kinetic and isotherm studies revealed that phosphate adsorption could be promoted by the functional interaction between Fe-PCC biochar and phosphate. Moreover, electrostatic interaction and intra particle diffusion might not play the main role in the mechanism of phosphate adsorption.

The FTIR results (Fig. 7d) showed that peaks at 1600, 1425, and 1090 cm^{-1} were preserved in PCC and shifted or decreased in Fe-PCC are absent from PO4@Fe-PCC (after reaction with phosphate) indicating that the functional groups (e.g., aromatic C=O, -CH_2, C–O–C) had reacted with phosphate. The peak at 1090 cm^{-1} disappeared and moved to 1150 cm^{-1} after the reaction with phosphate. Such peak is assigned to the stretching of hydrogen-bonded P=O of phosphates. Furthermore, a series of vibration peaks located at 780–1000 cm^{-1} were assigned to the asymmetric stretching vibrations of P–O–P and C–O–P. Compared with the results before the reaction with phosphate, the peak of Fe–O is reduced and shifted to 625 cm^{-1} indicating that the iron ions participate in phosphate adsorption as the hydroxyl group of was replaced by phosphate.

Based on XRD analysis the iron took the form of amorphous akaganeite phase in iron-loaded biochar, Fe-PCC, which represent excellent removal ability due to its high isoelectric point [49]. The modification of biochar with iron is an efficient and economical method to improve the adsorp-

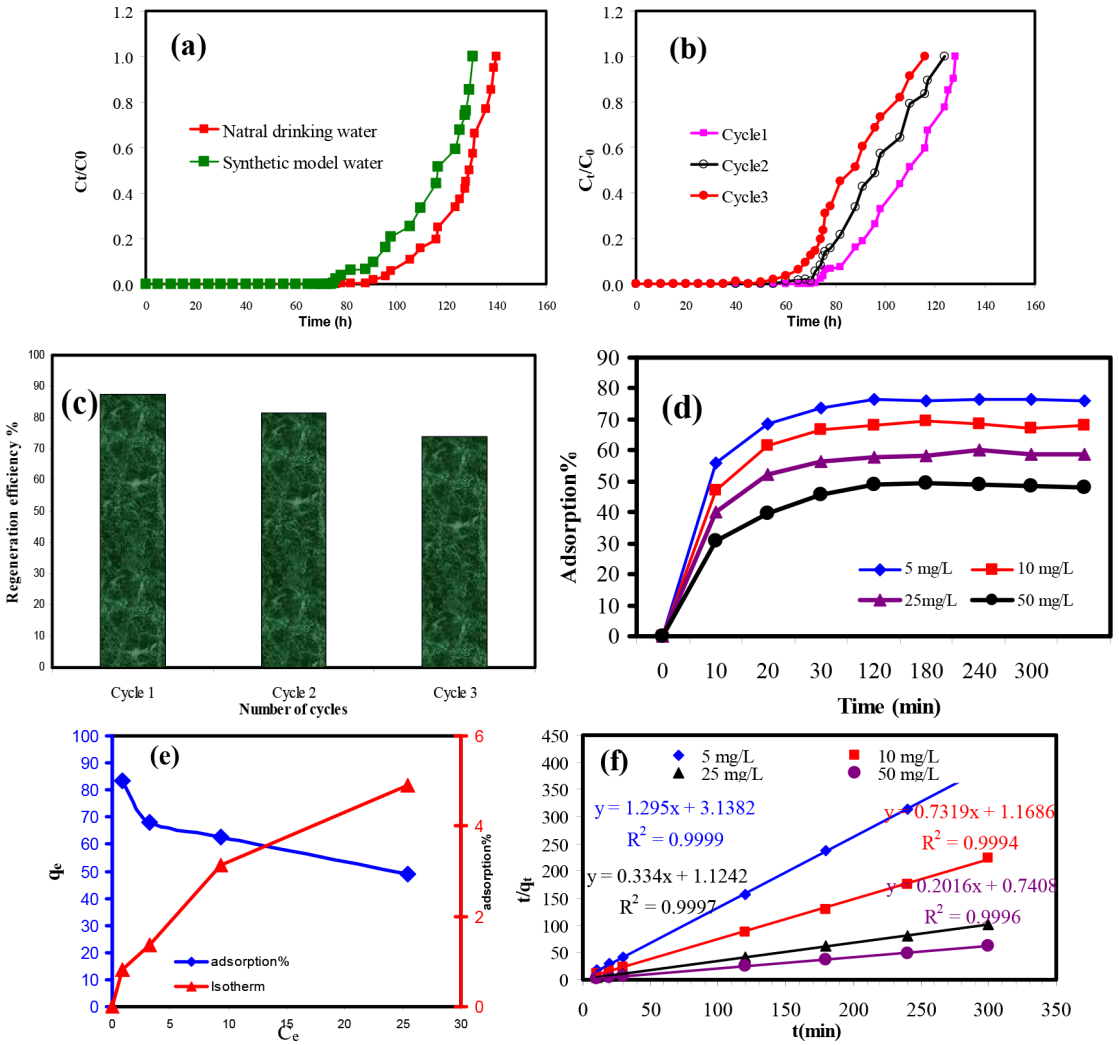

Fig. 9. Adsorption of phosphate using iron loaded palm biochar in fixed bed column and batch modes. Breakthrough curves: effect of water type (a), effect of regeneration and recycling on Fe-PCC bed (b) and influence of regeneration efficiency (%) by cycle number (c). In batch mode: effect of time (d), effect of initial iron concentration and isotherm (e) and pseudo-second order kinetic model (f).

Table 8
Column parameters of phosphate removal by Fe-PCC fixed bed from natural drinking water and model water

Water type	t_b (h)	t_e (h)	V_{eff}(L)	q_{total} (mg)	m_{total} (mg)	q_e (mg/g)	Y%
Model water	82.51	139.18	24.12	7.64	9.93	5.4	76.93
Natural drinking water	97.33	152.02	27.36	8.65	10.58	6.03	81.75

Table 9
Column parameters for Fe-PCC backed column, effect of regeneration

Cycle Number	t_b (h)	t_e (h)	V_{eff}(L)	q_{total} (mg)	m_{total} (mg)	q_e (mg/g)	RE%
Cycle 1	85.27	116.9	21.05	8.14	9.68	5.09	87.6
Cycle 2	79.35	130.84	23.67	7.57	9.36	4.73	81.52
Cycle 3	71.83	128.92	23.4	7.26	8.77	4.53	73.80

tion capacity of biochar [50,51]. The acting of iron modification mainly is to provide more attractive sites to biochar via changing the surface structure. Fe significantly decreased the negativity of the palm biochar surface charge through the formation of akaganeite. It was reported that the adsorption capacity of unmodified biochar for phosphate anions exhib-

Table 10
The kinetic parameters for phosphate adsorption by Fe-PCC biochar

C_0	q_e (mg/g) (experimental)	q_e (mg/g) (calculated)	Pseudo first-order	Pseudo second-order	Elovich	Intra particle diffusion
10 mg/L	0.83	0.77	K_1 = 0.004	K_2 = 0.534	α = 1996	K_{int} = 0.01
			R^2 = 0.583	R^2 = 0.999	β = 20.7	C = 0.62
					R^2 = 0.730	R^2 = 0.579
25 mg/L	1.37	1.37	K_1 = 1.923	K_2 = 0.458	α = 1254	K_{int} = 0.019
			R^2 =0.170	R^2 = 0.999	β = 10.76	C = 1.09
					R^2 = 0.635	R^2 = 0.476
50 mg/L	3.13	2.99	K_1 = 0.005	K_2 = 0.099	α = 735	K_{int} = 0.047
			R^2 =0.657	R^2 = 0.999	β = 4.52	C = 2.27
					R^2 = 724	R^2 =0.580
75 mg/L	4.92	4.96	K_1 = 0.010	K_2 = 0.055	α = 66	K_{int} = 0.010
			R^2 = 0.384	R^2 = 0.999	β = 2.16	C = 3.472
					R^2 = 0.788	R^2 = 0.6358

Table 11
The adsorption isotherm parameters of phosphate removal by Fe-PCC biochar

Langmuir		Freundlich		Temkin	
q_L	2.21	n	0.60	A	0.60
K_L	0.11	K_F	1.17	B	1.21
R_L	0.04				
R^2	0.37	R^2	0.98	R^2	0.92

ited much-reduced adsorption efficiency for removal compared to metal loaded biochar [52]. This was assigned to the function of electrostatic attraction force as one of phosphate removal mechanism [53] as repulsion between the negatively charged biochar surface and the phosphate ions could be the main reason for this observation. Therefore, the loading of biochar with iron improves the phosphate adsorption capability due to a decrease in negative surface charge.

Precipitation of phosphate anions with metals has been accepted as a mechanism for the adsorption of phosphate by biochars [54]. The complexation mechanism was supported by an increase in sorption solution pH during the adsorption process of phosphate [55]. Phosphate adsorption onto metal loaded biochar could involve also anion exchange [54]. However, the electrostatic attraction force is almost always an important step for biochars. This is obvious because the surface of biochar possesses some surface charge and phosphate is negatively charged.

Fig. 10 illustrates the major mechanisms that could be involved in phosphate adsorption by iron-loaded palm biochar, ligand exchange (outer and inner-sphere complexation), ion exchange, electrostatic attraction, precipitation, and others.

4. Conclusion

This study introduces a cost-effective and advantageous technique to remove iron from drinking groundwater. Successive adsorption was performed by using the spent iron-loaded biochar to remove phosphate from water samples. Using biochar in water treatment has many potential advantages compared to existing methods as biochar is a renewable and low-cost material which makes it suitable for poor communities such as Al Kharga. Four parts of palm trimming waste biochars were used to remove iron content from groundwater samples namely palm coir (PC), palm leaflets (PL), date empty bunches (DB) and date stone (DS). The breakpoint time and total adsorbed iron quantity decreased with the following sequence: PCC > DSC > DBC > PLC. The total absorbed iron mass and the maximum iron uptakes followed the

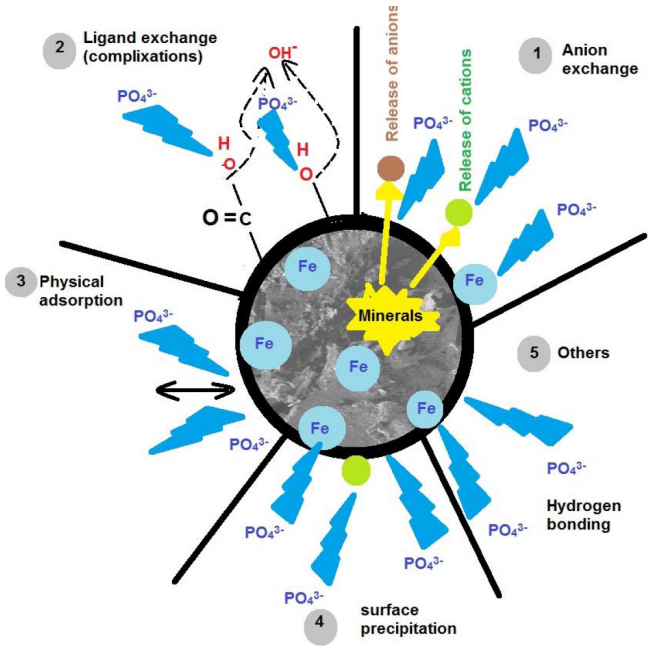

Fig. 10. Schematic illustration of phosphate adsorption using iron loaded palm biochar.

same order. Iron removal could be controlled by many processes because the correlation coefficient values of Langmuir, Freundlich and Temkin isotherms were close to one another. The phosphate adsorption are described by Freundlich isotherm model. The pseudo-second-order model has been observed to simulate iron and phosphate adsorption processes. In addition, results showed that no major decrease of regeneration efficiency was observed during the regeneration cycles which shows that the palm biochar has good potential to remove iron although it has been reused for a few times.

References

[1] V.K. Nguyen, Y. Ahn, Electrochemical removal and recovery of iron from groundwater using non-corrosive electrodes, J. Environ. Manage., 211 (2018) 36–41.
[2] K. Vaaramaa, J. Lehto, Removal of metals and anions from drinking water by ion exchange, Desalination, 155 (2003) 157–170.
[3] W.C. Andersen, T.J. Bruno, Application of a gas–liquid entraining rotor to supercritical fluid extraction: Removal of iron(III) from water, Anal. Chim. Acta, 485 (2003) 1–8.
[4] H.A. Aziz, M.S. Yusoff, M.N. Adlan, N.H. Adnan, S. Alias, Physico-chemical removal of iron from semi-aerobic landfill leachate by limestone filter, Waste Manage., 24 (2004) 353–358.
[5] D. Ellis, C. Bouchard, G. Lantagne, Removal of iron and manganese from groundwater by oxidation and micro filtration, Desalination, 130 (2000) 255–264.
[6] B.Y. Cho, Iron removal using an aerated granular filter, Process Biochem., 40 (2005) 3314–3320.
[7] S. Tahir, N. Rauf, Removal of Fe (II) from the wastewater of a galvanized pipe manufacturing industry by adsorption onto bentonite clay, J. Environ. Manage., 73 (2004) 285–292.
[8] B. Das, P. Hazarika, G. Saikia, H. Kalita, D.C. Goswami, H.B. Das, S.N. Dube, R.K. Dutta, Removal of iron from groundwater by ash: A systematic study of a traditional method, J. Hazard. Mater., 141 (2007) 834–834.
[9] C. Prochaska, A. Zouboulis, Removal of phosphates by pilot vertical-flow constructed wetlands using a mixture of sand and dolomite as substrate, Ecol. Eng., 26 (2006) 293–303.
[10] D. Zhao, A.K. Sengupta, Ultimate removal of phosphate from wastewater using a new class of polymeric ion exchangers, Water Res., 32 (1998) 1613–1625.
[11] P.E. Lamoreaux, B.A. Memon, H. Idris, Groundwater development, Kharga Oases, Western Desert of Egypt: A long-term environmental concern, Environ. Geol. Water Sci., 7 (1985) 129–149.
[12] A.M. Ebraheem, S. Riad, P. Wycisk, A.M.S. El Nasr, Simulation of impact of present and future groundwater extraction from the non-replenished Nubian Sandstone Aquifer in SW Egypt, Environ. Geol., 43 (2002) 188–196.
[13] W.E. Mahmod, K. Watanabe, A.A. Zahr-Eldeen, Analysis of groundwater flow in arid areas with limited hydrogeological data using the Grey Model: a case study of the Nubian Sandstone, Kharga Oasis, Egypt, Hydrogeol. J., 21 (2013) 1021–1034.
[14] W.E. Mahmod, K. Watanabe, Modified grey model and its application to groundwater flow analysis with limited hydrogeological data: a case study of the Nubian Sandstone, Kharga Oasis, Egypt. Environ. Monit. Assess., 186 (2014) 1063–1081.
[15] M. Gad, K. Dahab, H. Ibrahim, Impact of iron concentration as a result of groundwater exploitation on the Nubian sandstone aquifer in El Kharga Oasis, western desert, Egypt, NRIAG-JAG (2016) doi:10.1016/j.nrjag.2016.04.003.
[16] Environmental action Plan New Valley Governorate, State Ministry of Environment - EEAA (2008).
[17] H.H. Sait, A. Hussain, A.A. Salema, F.N. Ani, Pyrolysis and combustion kinetics of date palm biomass using thermogravimetric analysis, Bioresour. Technol., 118 (2012) 382–389.
[18] D.Z. Husein, Adsorption and removal of mercury ions from aqueous solution using raw and chemically modified Egyptian mandarin peel, Desal. Water Treat., 51 (2013) 6761–6769.
[19] M. Ehsan, M.A. Barakat, D.Z. Husein, S.M. Ismail, Immobilization of Ni and Cd in soil by biochar derived from unfertilized dates, Water Air Soil Pollut., (2014) 2125–2123.
[20] H. Kehl, R. Bornkamm, Landscape ecology and vegetation units of the western desert of Egypt. In B. Meissner, P. Wycisk (Eds.) Geopotential ecology: analysis of a desert region. Catena Suppl., 26 (1993) 155–178.
[21] APHA, AWWA, WPCF, Standard methods for the examination of water and wastewater (18th ed.), American Public Health Association, Washington, USA, 1992.
[22] D.Z. Husein, E. Aazam, M. Battia, Adsorption of cadmium(II) onto watermelon rind under microwave radiation and application into surface water from Jeddah, Saudi Arabia. Arab, J. Sci. Eng., 42 (2017) 2403–2415.
[23] R.A. Nasser, An evaluation of the use of midribs from common date palm cultivars grown in Saudi Arabia for energy production, Bio. Resour., 9 (2014) 4343–4357.
[24] WHO: WHO Guidelines for drinking water quality. First Addendum to 3rd ed., Geneva, 2006.
[25] V. Premlata, Multivariant analysis of drinking water quality parameters of lake Pichhola in Udaipur. India, Biol. Forum Int J., 1 (2009) 97–102.
[26] R. Udhayakumar, P. Manivannan, K. Raghu, S. Vaideki, Assessment of physico-chemical characteristics of water in Tamilnadu, Ecotoxicol. Environ. Saf., 134 (2016) 474–477.
[27] R. Han, L. Zou, X. Zhao, Y. Xu, F. Xu, Y. Li, Y. Wang, Characterization and properties of iron oxide-coated zeolite as adsorbent for removal of copper(II) from solution in fixed bed column, Chem. Eng. J., 149 (2009) 123–131.
[28] E. Oguz, M. Ersoy, Removal of Cu^{2+} from aqueous solution by adsorption in a fixed bed column and neural network modeling, Chem. Eng. J., 164 (2010) 56–62.
[29] D.Z. Husein, T. Al-Radadi, E.Y. Danish, Adsorption of phosphate using alginate-/zirconium-grafted newspaper pellets: fixed-bed column study and application, Arab. J. Sci. Eng., 42 (2016) 1399–1412.
[30] S. Lagergern, About the theory of so-called adsorption of soluble substances, K. Sven. Vetenskapsakad. Handl., 24 (1898) 1–39.
[31] G. Mckay, Y.S. Ho, Psuedo-second order model for sorption processes, Process. Biochem., 34 (1999) 451–465.
[32] W.J. Weber, J.C. Morris, Kinetics of adsorption on carbon from solution, J. Sanit. Eng. Div. Proc. Am. Soc. Civil. Eng., 89 (1963) 31–59.
[33] W. Weber, J. Morris, Kinetics of adsorption on carbon from solution, J. Sanit. Eng. Div., 89 (1963) 31–60.
[34] I. Langmuir, The adsorption of gases on plane surfaces of glass, mica and platinum, J. Am. Chem. Soc., 40 (1918) 1361–1403.
[35] H.M.F. Freundlich, Uber die adsorption in Losungen [Over the adsorption in solution], Z. Phys. Chem., 57 (1906) 385–470.
[36] M.I. Temkin, V. Pyzhev, Kinetics of ammonia synthesis on promoted iron catalysts, Acta Physicochim., USSR, 12 (1940) 217–222.
[37] E.A. Da Silva, E.S. Cossich, C.R.G. Tavares, L.C. Filho, R. Guirardello, Modeling of copper(II) biosorption by marine alga Sargassum sp. in fixed-bed column, Process Biochem., 38 (2002) 791–799.
[38] C.A. Henriques, A.C.A. da Costa, M.M. dos Reis, A.L.H. Costa, A.S. Luna, Batch and fixed-bed column biosorption of manganese ion by Sargassum filipendula, Electron. J. Biotechnol., 14 (2011) 8–8.
[39] A. Shahbazi, H. Younesi, A. Badiei, Batch and fixed-bed column adsorption of Cu(II), Pb(II) and Cd(II) from aqueous solution onto functionalised SBA-15 mesoporous silica, Can. J. Chem. Eng., 91 (2013) 739–750.
[40] M. Jang, W. Chen, F.S. Cannon, Preloading hydrous ferric oxide into granular activated carbon for arsenic removal, Environ. Sci. Technol., 42 (2008) 3369–3374.
[41] M. Şener, B. Kayan, S. Akay, B. Gözmen, D. Kalderis, Fe-modified sporopollenin as a composite biosorbent for the removal of Pb^{2+} from aqueous solutions, Desal. Water Treat., 3994 (2016) 1–19.
[42] S.S. Mayakaduwa, P. Kumarathilaka, I. Herath, M. Ahmad, M. Al-Wabel, Y.S. Ok, A. Usman, A. Abduljabbar, M. Vithanage,

Equilibrium and kinetic mechanisms of woody biochar on aqueous glyphosate removal, Chemosphere, 144 (2016) 2516–2521.
[43] M. Uchimiya, I.M. Lima, K.T. Klasson, S. Chang, L.H. Wartelle, J.E. Rodgers, Immobilization of heavy metal ions (CuII, CdII, NiII, and PbII) by broiler litter-derived biochars in water and soil, J. Agric. Food Chem., 58 (2010) 5538–5544.
[44] P. Nautiyal, K.A. Subramanian, M.G. Dastidar, Adsorptive removal of dye using biochar derived from residual algae after in-situ transesterification: alternate use of waste of biodiesel industry, J. Environ. Manage., 182 (2016) 187–197.
[45] S. Fan, J. Tang, Y. Wang, H. Li, H. Zhang, J. Tang, Z. Wang, X. Li, Biochar prepared from co-pyrolysis of municipal sewage sludge and tea waste for the adsorption of methylene blue from aqueous solutions: kinetics, isotherm, thermodynamic and mechanism, J. Mol. Liq., 220 (2016) 432–441.
[46] X. Cao, W. Harris, Properties of dairy-manure-derived biochar pertinent to its potential use in remediation, Bioresour. Technol., 101 (2010) 5222–5228.
[47] S. Fan, J. Tang, Y. Wang, H. Li, H. Zhang, J. Tang, Z. Wang, X. Li, Biochar prepared from co-pyrolysis of municipal sewage sludge and tea waste for the adsorption of methylene blue from aqueous solutions: Kinetics, isotherm, thermodynamic and mechanism, J. Mol. Liq., 220 (2016) 432–441.
[48] M. Keiluweit, M. Kleber, Molecular-level interactions in soils and sediments: the role of aromatic p-systems, Environ. Sci. Technol., 43 (2009) 3421–3429.
[49] M.L. Pierce, C.B. Moore, Adsorption of arsenite and arsenate on amorphous iron hydroxide, Water Res., 16 (1982) 1247–1253.
[50] Q. Yang, X. Wang, W. Luo, J. Sun, Q. Xu, F. Chen, J. Zhao, S. Wang, F. Yao, D. Wang, X. Li, G. Zeng, Effectiveness and mechanisms of phosphate adsorption on iron-modified biochars derived from waste activated sludge, Bioresour. Technol., 247 (2018) 537–544.
[51] J. Ren, N. Li, L. Li, J.K. An, L. Zhao, N.Q. Ren, Granulation and ferric oxides loading enable biochar derived from cotton stalk to remove phosphate from water, Bioresour. Technol., 178 (2015) 119–125.
[52] Z. Wang, D. Shen, F. Shen, T. Li, Phosphate adsorption on lanthanum loaded biochar, Chemosphere, 150 (2016) 1–7.
[53] W. Ding, X. Dong, I.M. Ime, B. Gao, L.Q. Ma, Pyrolytic temperatures impact lead sorption mechanisms by bagasse biochars, Chemosphere, 62 (2014) 1912–1918.
[54] D.L. Sparks, Environmental soil chemistry. 2nd ed. Academic Press, New York. 2003.
[55] S. Wan, S. Wang, Y. Li, B. Gao, Functionalizing biochar with Mg-Al and Mg-Fe layered double hydroxides for removal of phosphate from aqueous solutions, J. Ind. Eng. Chem., 47 (2017) 246–253.